

## Supporting Information

### Synthesis and characterization of open and sandwich-type polyoxometalates reveals visible-light-driven water oxidation via POM-photosensitizer complexes

Pierre-Emmanuel Car,<sup>\*a</sup> Miguel Guttentag,<sup>a</sup> Kim K. Baldrige,<sup>b</sup> Roger Alberto,<sup>a</sup>  
Greta R. Patzke<sup>\*a</sup>

<sup>a</sup>Institute of Inorganic Chemistry, University of Zurich, Winterthurerstrasse 190, CH-8057 Zurich, Switzerland.

<sup>b</sup>Institute of Organic Chemistry, University of Zurich, Winterthurerstrasse 190, CH-8057 Zurich, Switzerland.

Corresponding author: Tel: +41 44 635 491; Fax: +41 44 635 6802; E-mail: [greta.patzke@aci.uzh.ch](mailto:greta.patzke@aci.uzh.ch)

#### Contents

1. Thermogravimetric analysis	2
2. FT-IR spectroscopy	4
3. Raman spectroscopy	6
4. UV/vis spectroscopy	8
5. Electrochemical characterizations	9
6. Electrospray ionization mass spectrometry	13
7. Visible light driven water oxidation	15
8. References	23

## 1. Thermogravimetric analysis (TGA)

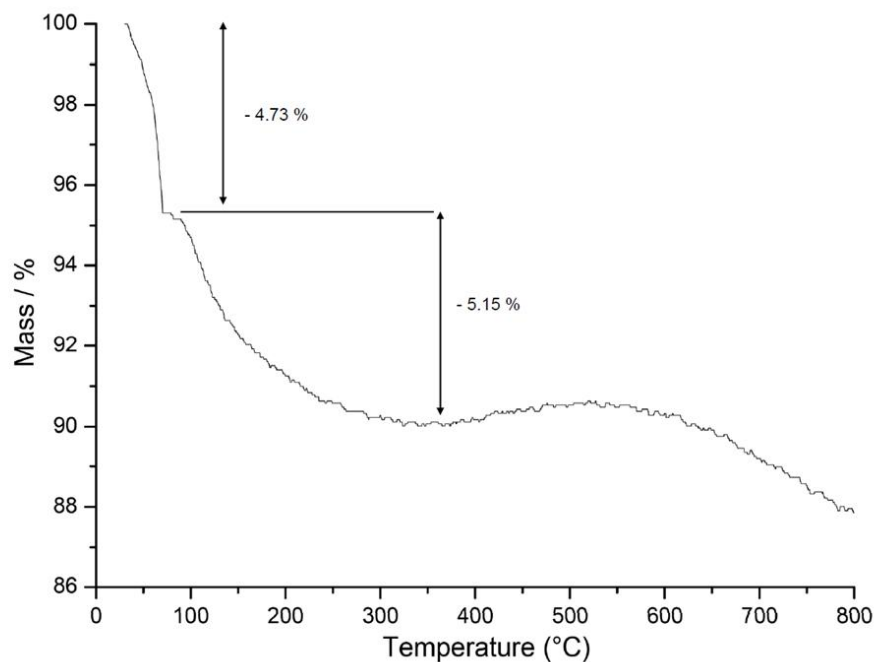


**Figure S1.** Thermogravimetric plot of  $\alpha\text{-K}_6\text{Na}[\{\text{Ru}_3\text{O}_3(\text{H}_2\text{O})\text{Cl}_2\}(\text{SiW}_9\text{O}_{34})]\cdot 17\text{H}_2\text{O}$  (**1**) (air,  $\text{Al}_2\text{O}_3$  crucible, heating rate: 5 K/min).

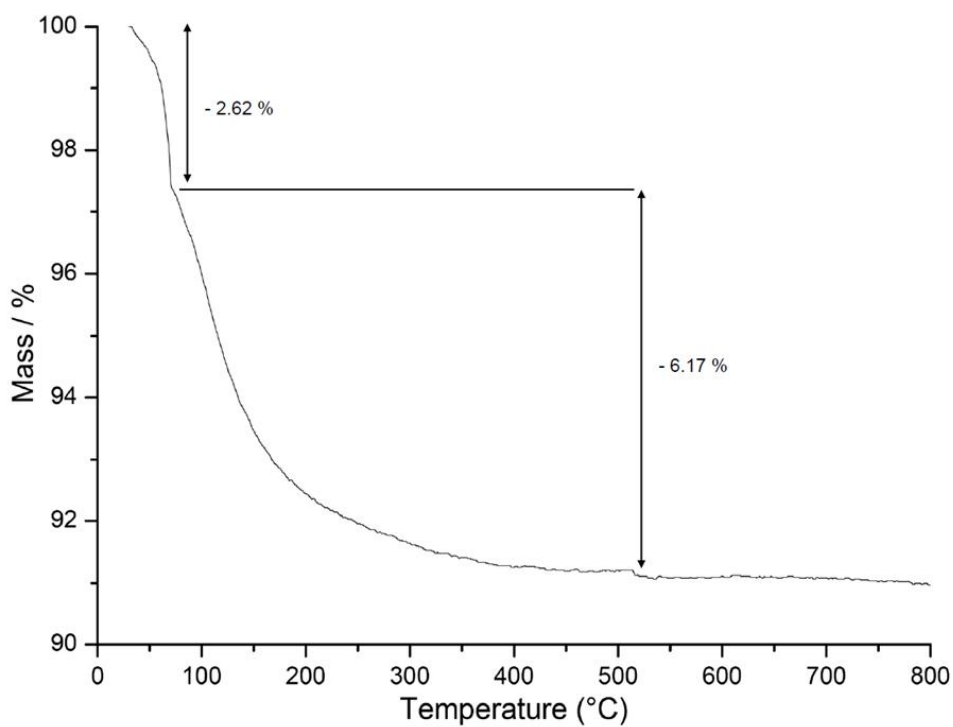


**Figure S2.** Thermogravimetric plot of  $\alpha\text{-K}_{11}\text{Na}_1[\text{Co}_4(\text{H}_2\text{O})_2(\text{SiW}_9\text{O}_{34})_2]\cdot 26\text{H}_2\text{O}$  (**2**) (air,  $\text{Al}_2\text{O}_3$  crucible, heating rate: 5 K/min).

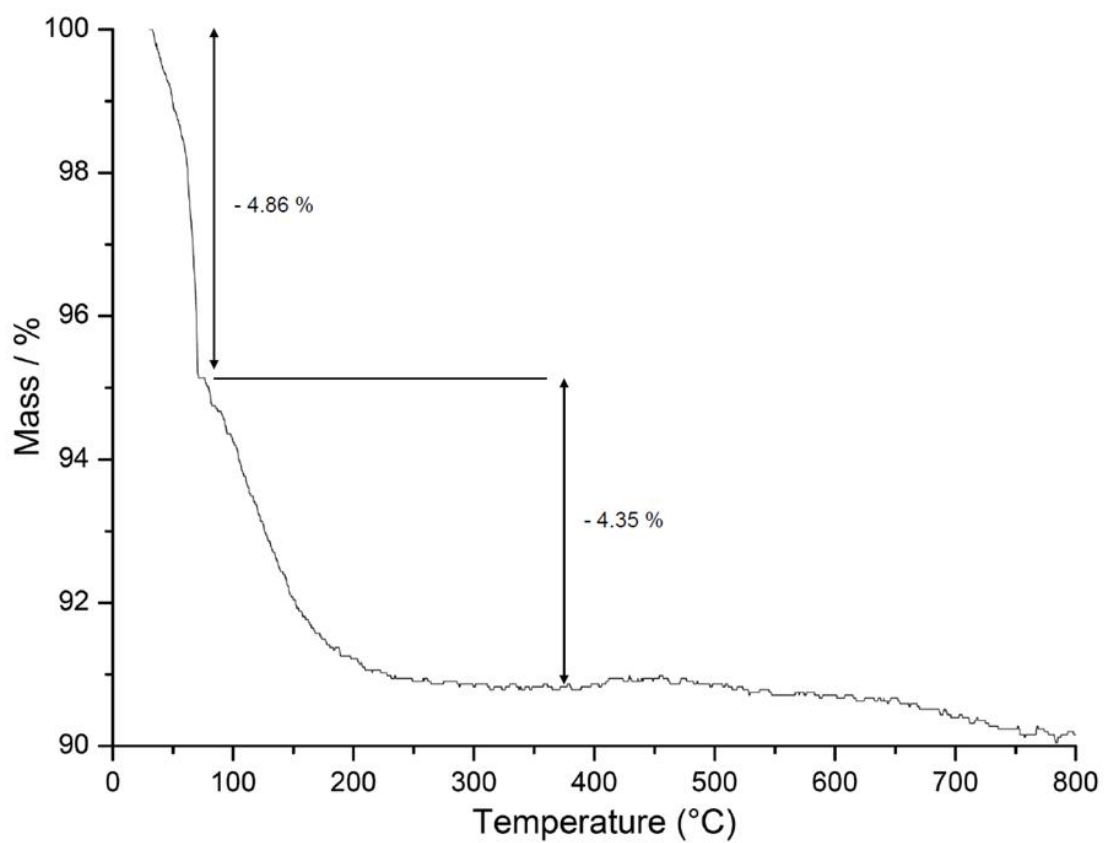


**Figure S3.** Thermogravimetric plot of  $\alpha$ -K<sub>11</sub>Na<sub>1</sub>[Ni<sub>4</sub>(H<sub>2</sub>O)<sub>2</sub>(SiW<sub>9</sub>O<sub>34</sub>)<sub>2</sub>] $\cdot$ 27H<sub>2</sub>O (**3**) (air, Al<sub>2</sub>O<sub>3</sub> crucible, heating rate: 5 K/min).

## 2. FT-IR spectroscopy

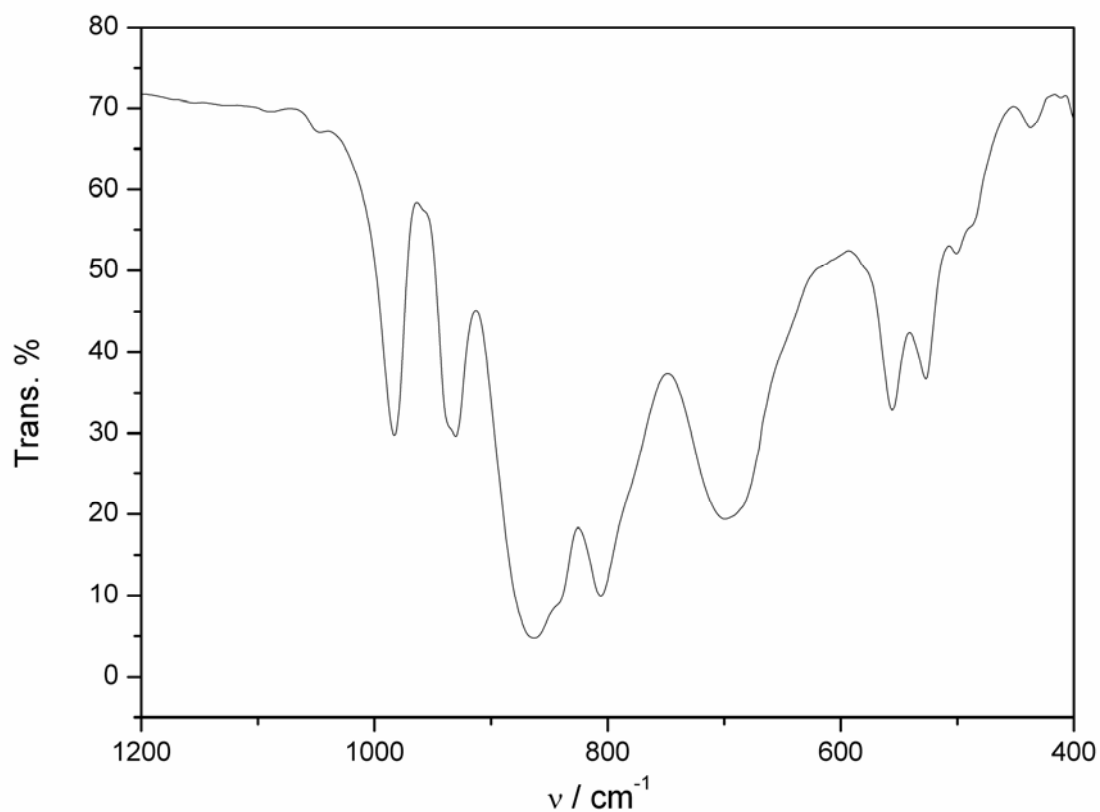


**Figure S4.** FT-IR spectrum of  $\alpha\text{-Na}_{10}[\text{SiW}_9\text{O}_{34}] \cdot 15\text{H}_2\text{O}$ .

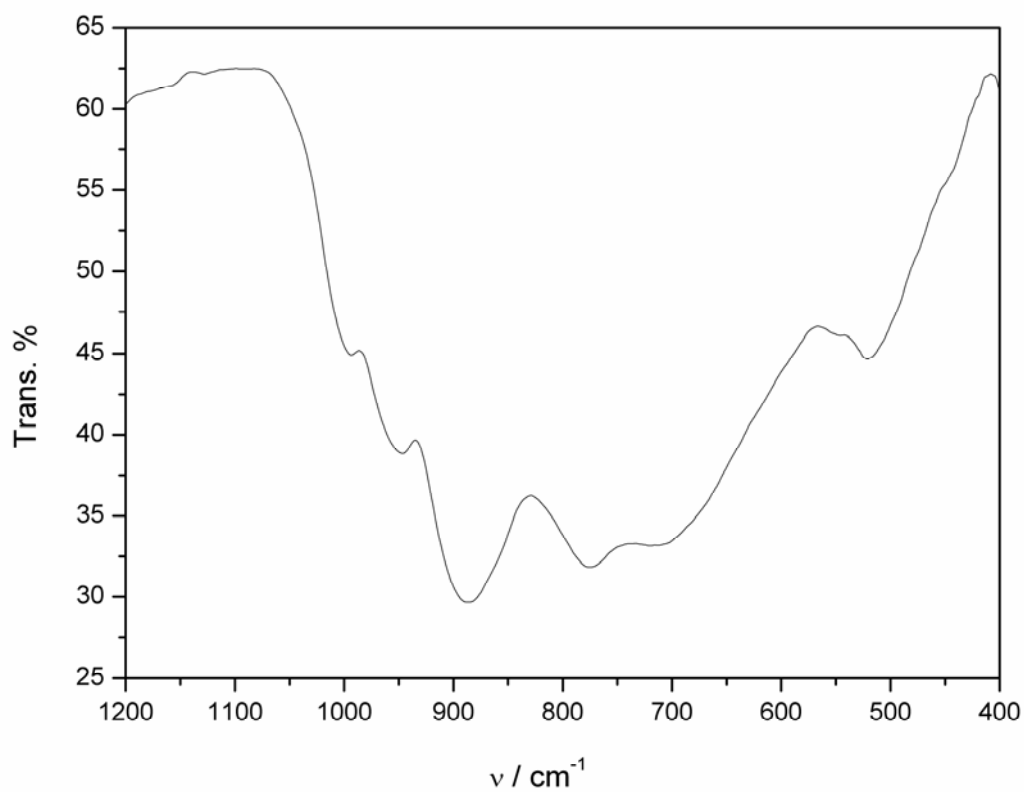


**Figure S5.** FT-IR spectrum of  $\alpha\text{-K}_6\text{Na}[\{\text{Ru}_3\text{O}_3(\text{H}_2\text{O})\text{Cl}_2\}(\text{SiW}_9\text{O}_{34})] \cdot 17\text{H}_2\text{O}$  (1).

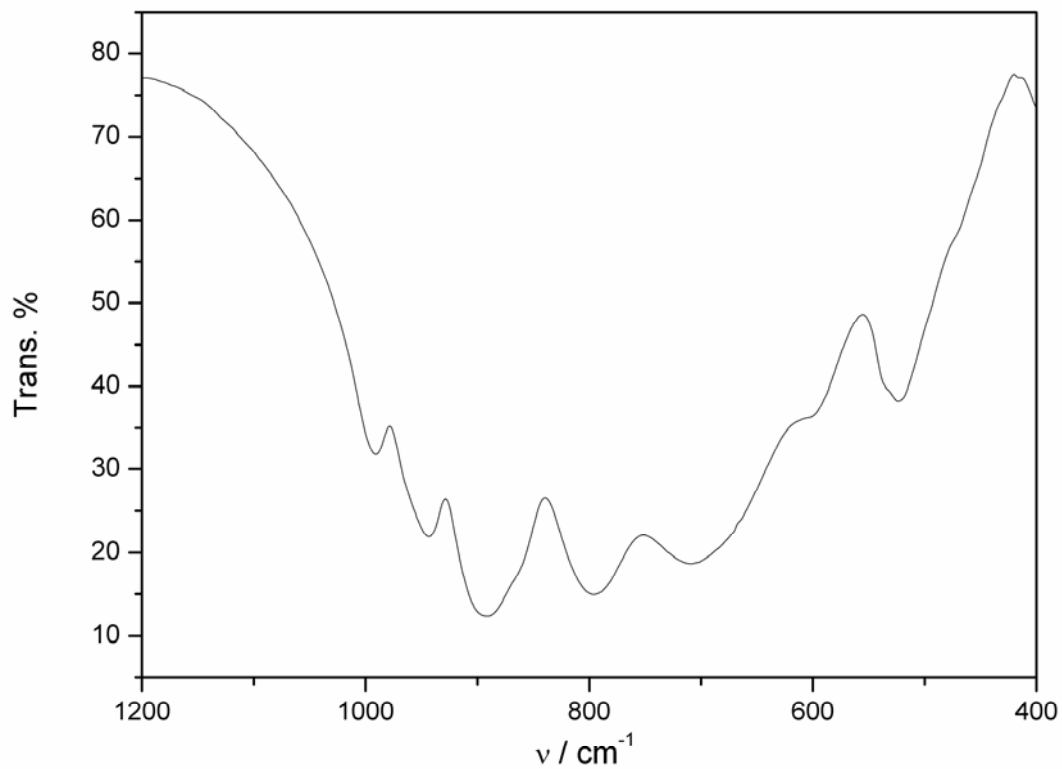


**Figure S6.** FT-IR spectrum of  $\alpha$ -K<sub>11</sub>Na<sub>1</sub>[Co<sub>4</sub>(H<sub>2</sub>O)<sub>2</sub>(SiW<sub>9</sub>O<sub>34</sub>)<sub>2</sub>] $\cdot$ 26H<sub>2</sub>O (**2**).

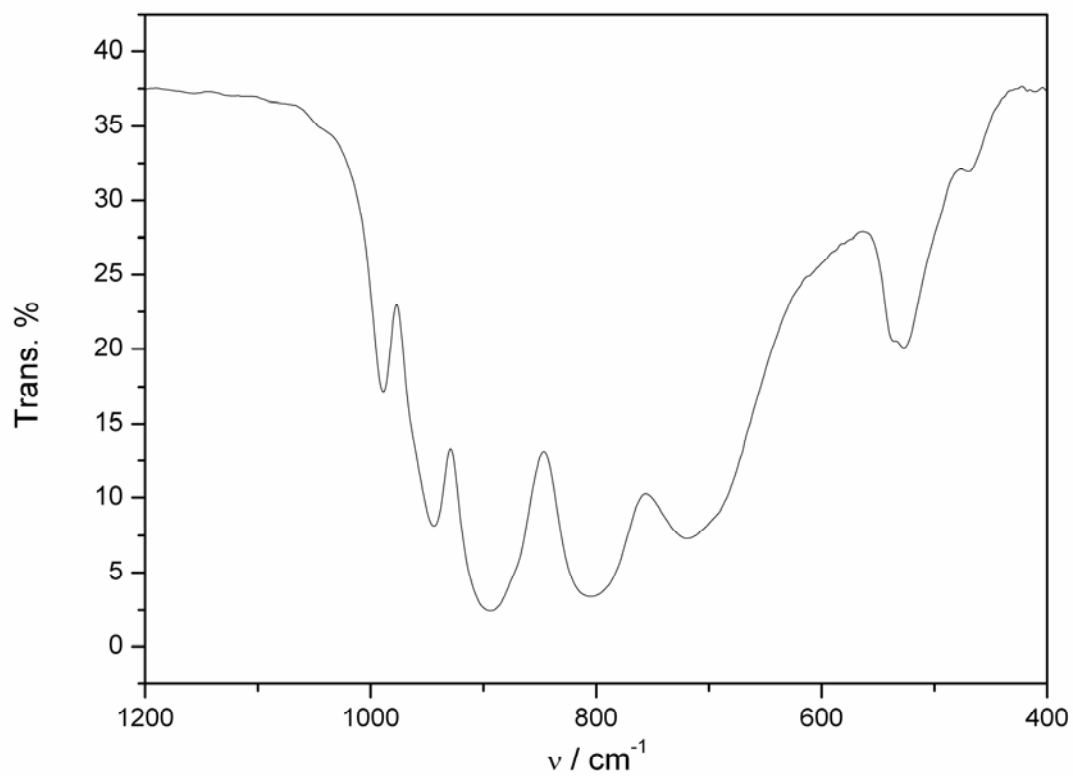


**Figure S7.** FT-IR Spectrum (KB pellet) of  $\alpha$ -K<sub>11</sub>Na<sub>1</sub>[Ni<sub>4</sub>(H<sub>2</sub>O)<sub>2</sub>(SiW<sub>9</sub>O<sub>34</sub>)<sub>2</sub>] $\cdot$ 27H<sub>2</sub>O (**3**).

### 3. Raman spectroscopy

Raman spectra were recorded on a Renishaw Ramascope spectrometer equipped with a laser diode working at 514 nm for the compound **(1)** and 715 nm for compounds **(2)** and **(3)**. Compound **(1)** was characterized as a concentrated liquid sample. Compounds **(2)** and **(3)** were characterized as solid samples.

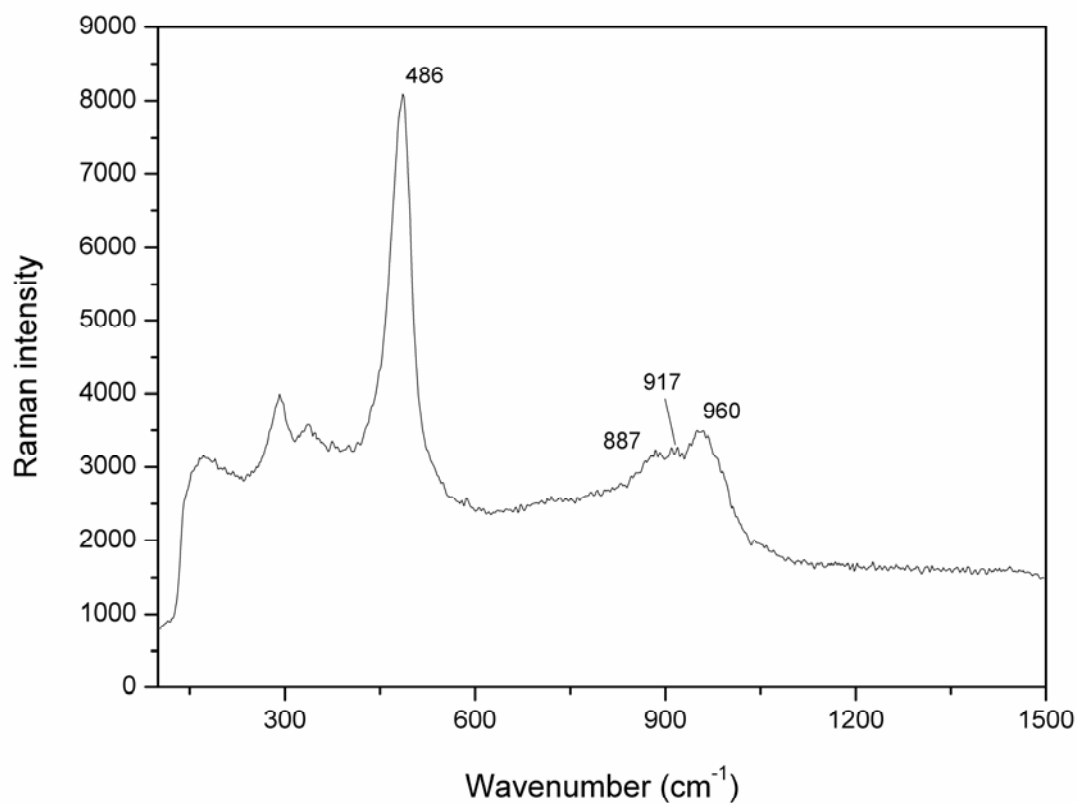


**Figure S8.** Raman spectrum of a concentrated aqueous solution of  $\alpha$ - $\text{K}_6\text{Na}[\{\text{Ru}_3\text{O}_3(\text{H}_2\text{O})\text{Cl}_2\}(\text{SiW}_9\text{O}_{34})] \cdot 17\text{H}_2\text{O} (**1**) displaying the characteristic  $\nu(\text{W}=\text{O})$  band at  $960\text{ cm}^{-1}$ .$

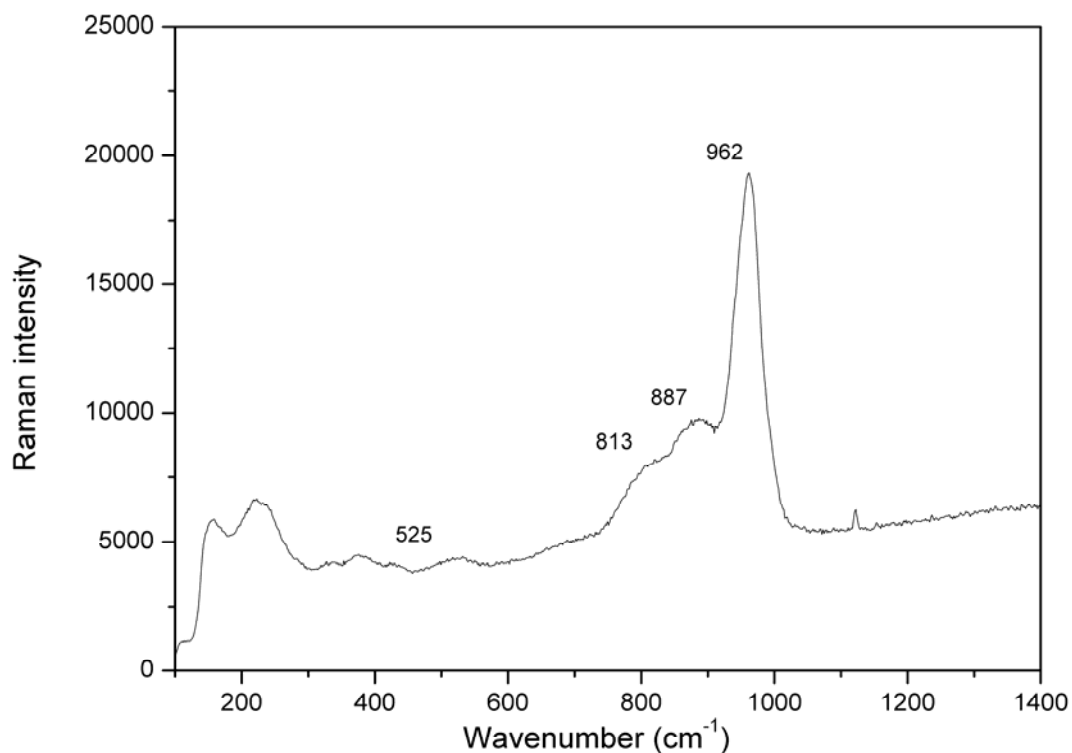


**Figure S9.** Solid-state Raman spectrum of  $\alpha\text{-K}_{11}\text{Na}_1[\text{Co}_4(\text{H}_2\text{O})_2(\text{SiW}_9\text{O}_{34})_2]\cdot 26\text{H}_2\text{O}$  (**2**) exhibiting the characteristic  $\nu(\text{W}=\text{O})$  band at  $962\text{ cm}^{-1}$ .

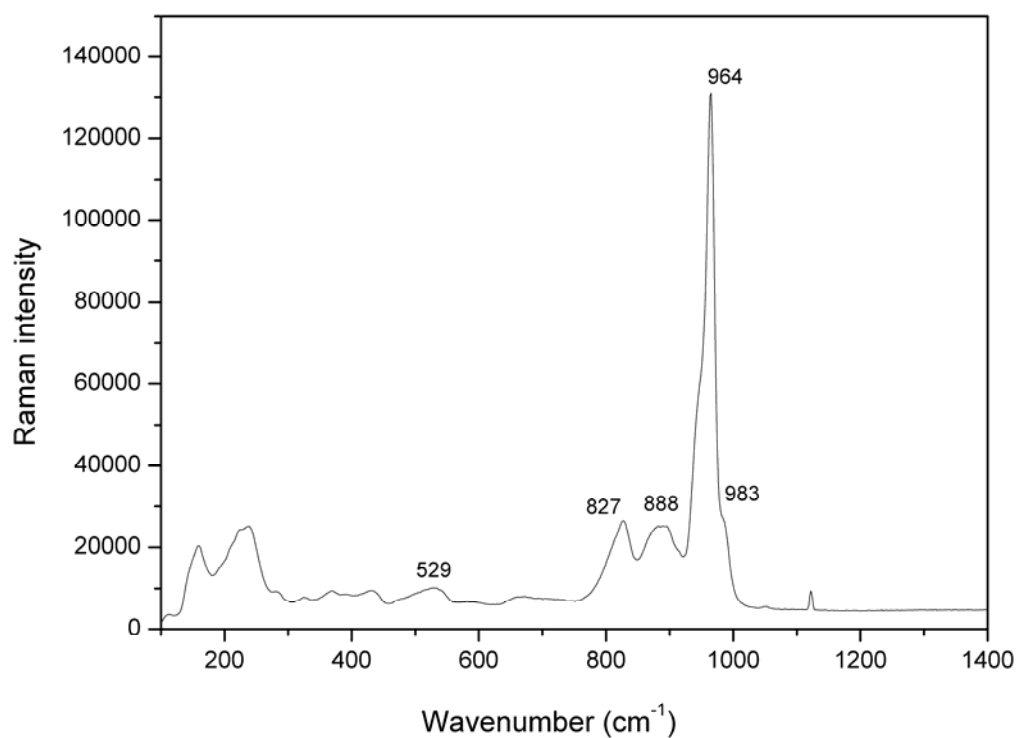


**Figure S10.** Solid-state Raman spectrum of  $\alpha\text{-K}_{11}\text{Na}_1[\text{Ni}_4(\text{H}_2\text{O})_2(\text{SiW}_9\text{O}_{34})_2]\cdot 27\text{H}_2\text{O}$  (**3**) exhibiting the characteristic  $\nu(\text{W}=\text{O})$  band at  $964\text{ cm}^{-1}$ .

#### 4. UV/vis absorption spectra

UV/vis spectra were recorded with a Lambda 650 S Perkin Elmer UV-Visible spectrometer in the 300-800 nm range using a Quartz SUPRASIL precision cell (10 mm).

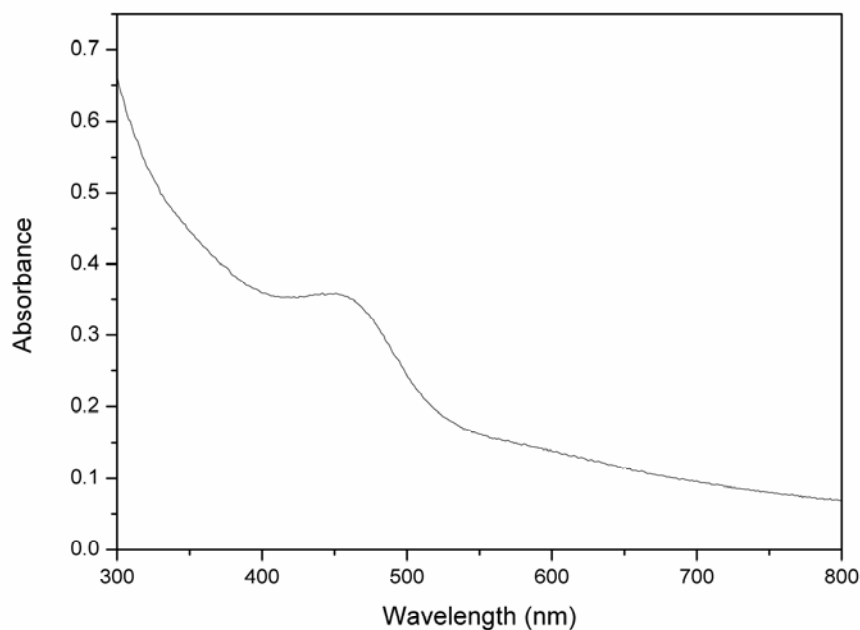


**Figure S11.** UV/vis absorption spectrum in solution ( $0.5 \cdot 10^{-5}$  M) of  $\alpha$ - $\text{K}_6\text{Na}[\{\text{Ru}_3\text{O}_3(\text{H}_2\text{O})\text{Cl}_2\}(\text{SiW}_9\text{O}_{34})] \cdot 17\text{H}_2\text{O}$  (**1**).

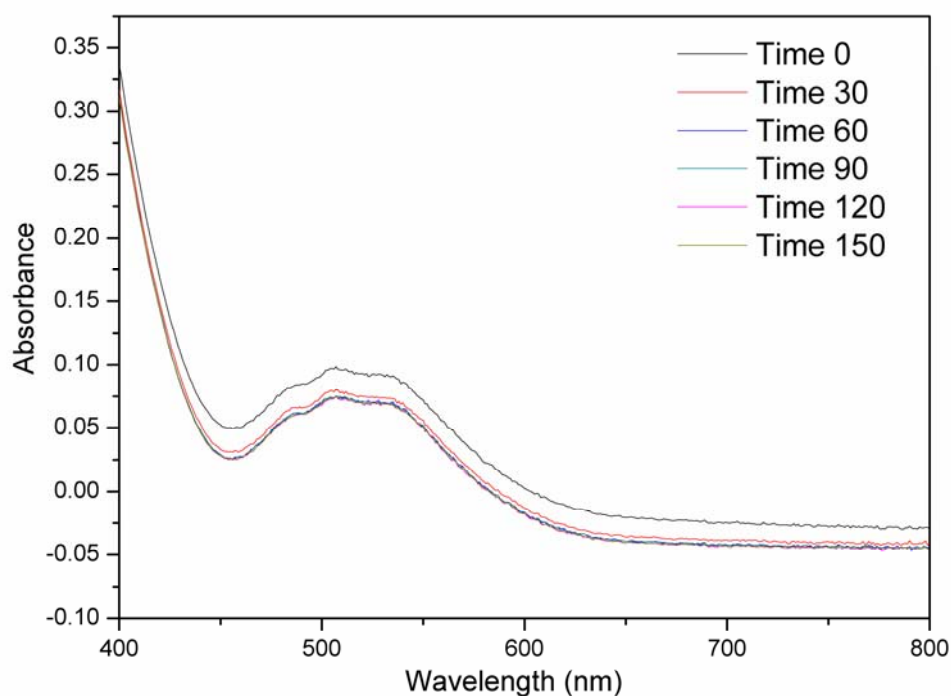


**Figure S12.** Time-dependent UV/vis absorption spectra of  $\alpha$ - $\text{K}_{11}\text{Na}_1[\text{Co}_4(\text{H}_2\text{O})_2(\text{SiW}_9\text{O}_{34})_2] \cdot 26\text{H}_2\text{O}$  (**2**) (1.06 mM) over 150 min in  $\text{Na}_2\text{SiF}_6$  buffer (20 mM, pH 5.8).

## 5. Electrochemical characterizations

All voltammograms were recorded on a Metrohm 797 VA Computrace instrument. The solutions were deaerated thoroughly for at least 10 min with pure N<sub>2</sub> and all experiments were performed at room temperature. A glassy carbon electrode (Metrohm AG, 3 mm diameter) was used as working electrode and all potentials were quoted to the Ag/AgCl reference electrode. The glassy carbon electrode was polished after each new measurement.

The cyclic voltammograms of **(1)**, **(2)** and **(3)** recorded at various pH values and in various media display the according redox waves of the different metallic centers. The potential domain of the voltammograms is divided into a positive and a negative section (vs. Ag/AgCl) for their sequential analysis.

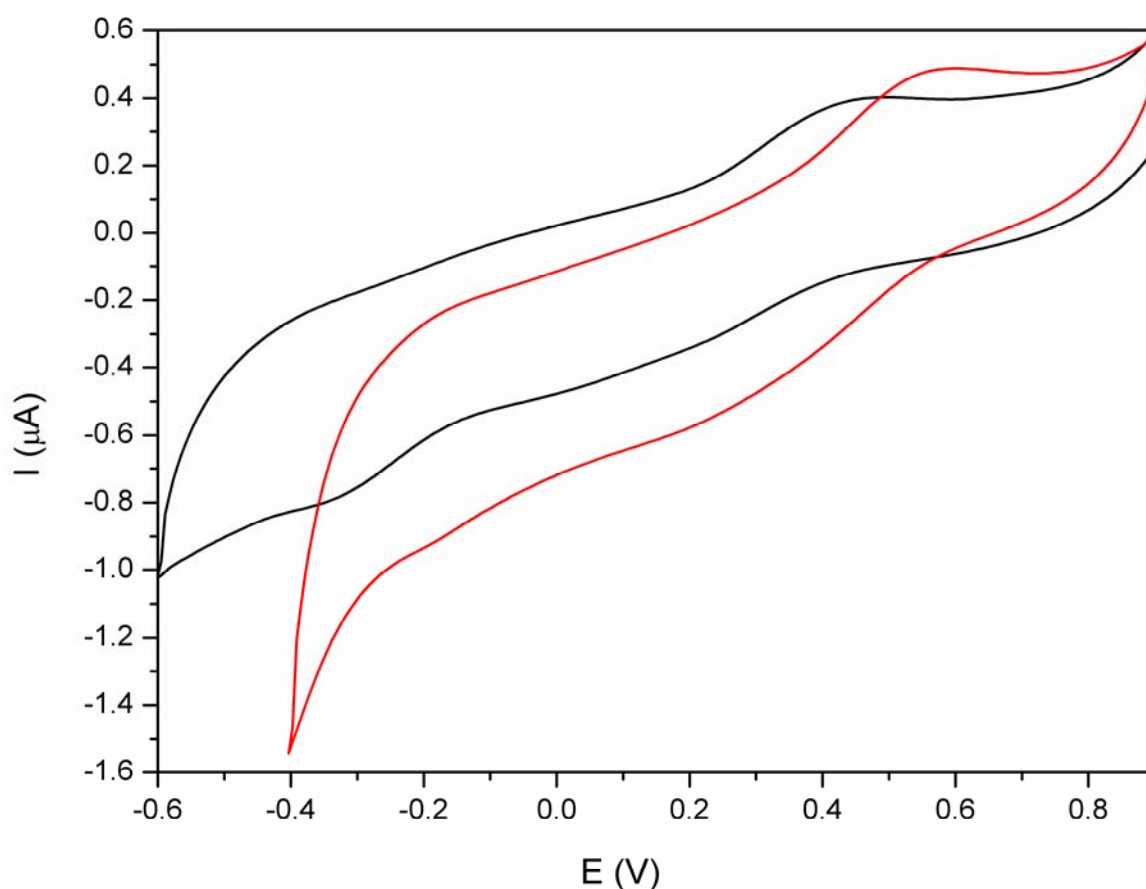


**Figure S13.** Cyclic voltammograms of  $\alpha\text{-K}_6\text{Na}[\{\text{Ru}_3\text{O}_3(\text{H}_2\text{O})\text{Cl}_2\}(\text{SiW}_9\text{O}_{34})]\cdot 17\text{H}_2\text{O}$  (**1**) (0.25 mM) for pH 3 (black line) and pH 1 (red line) in sulfate buffer; scan rate: 25 mV/s.

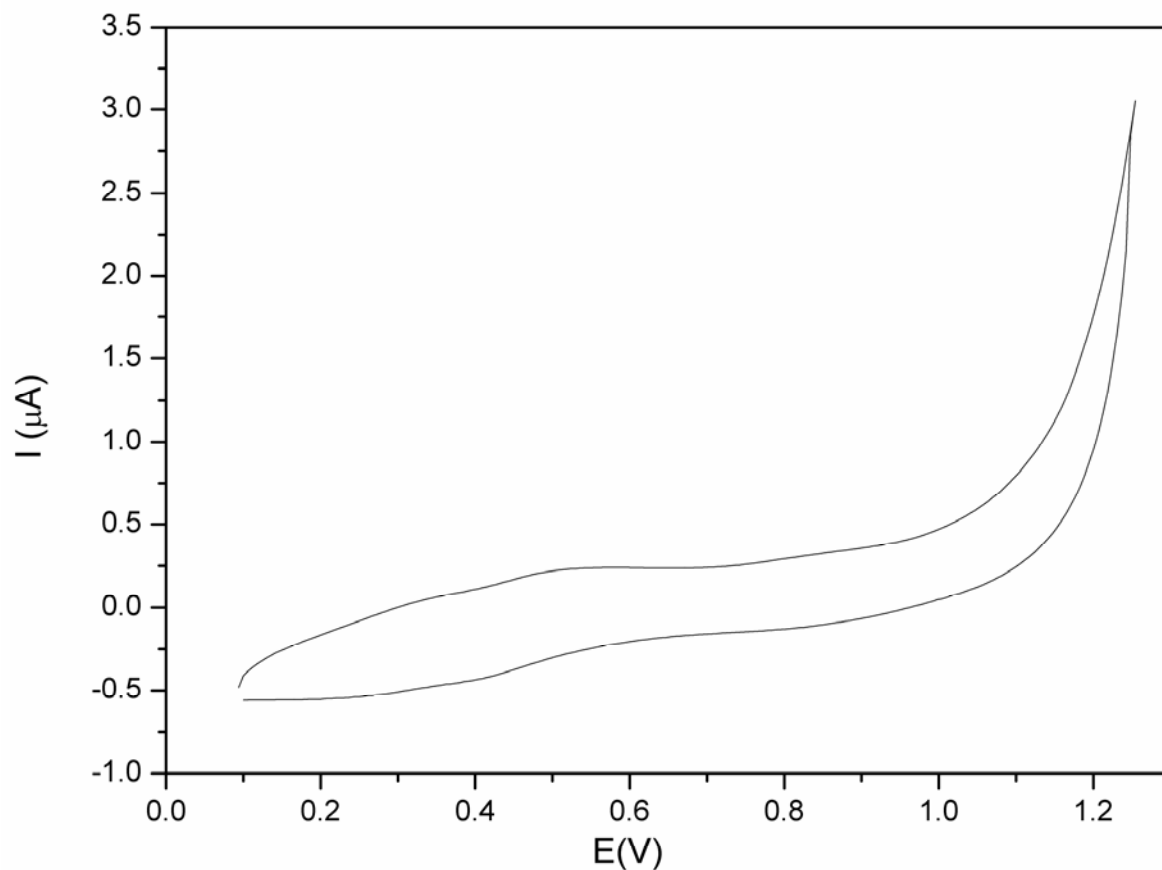


**Figure S14.** Cyclic voltammograms of  $\alpha\text{-K}_6\text{Na}[\{\text{Ru}_3\text{O}_3(\text{H}_2\text{O})\text{Cl}_2\}(\text{SiW}_9\text{O}_{34})]\cdot 17\text{H}_2\text{O}$  (**1**) (0.25 mM) at pH 1 in sulfate buffer; scan rate: 25 mV/s. Insert: enlarged voltammogram of the positive potential domain.

POM (**1**) recorded in  $\text{Na}_2\text{SO}_4$  solution (pH = 1 and 3) displays one pair of redox peaks in the positive domain and an corresponding pair in the negative domain that are attributed to the  $\text{Ru}^{\text{V}}/\text{Ru}^{\text{IV}}$ ,  $\text{Ru}^{\text{IV}}/\text{Ru}^{\text{III}}$  and  $\text{Ru}^{\text{III}}/\text{Ru}^{\text{II}}$  redox processes, respectively. Values less defined around +0.70 to +0.87 V for  $\text{Ru}^{\text{V}}/\text{Ru}^{\text{IV}}$ , values around +0.32 to +0.54 V for  $\text{Ru}^{\text{IV}}/\text{Ru}^{\text{III}}$  and around -0.12 to -0.22 V for  $\text{Ru}^{\text{III}}/\text{Ru}^{\text{II}}$  are in good agreement with reported results<sup>1</sup> for a ruthenium Keggin type polyoxometalate and with other related compounds.<sup>2,1b</sup>

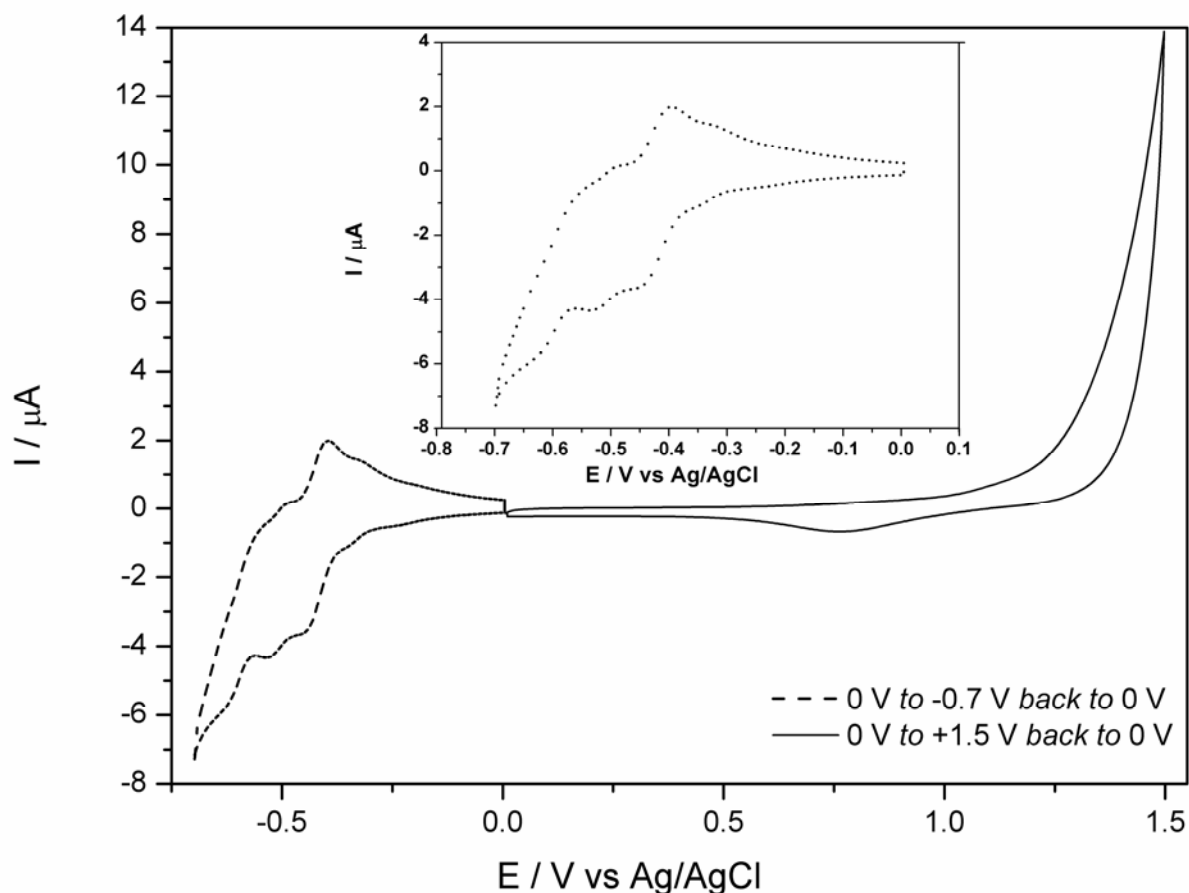


**Figure S15.** Cyclic voltammograms of  $\alpha\text{-K}_{11}\text{Na}_1[\text{Co}_4(\text{H}_2\text{O})_2(\text{SiW}_9\text{O}_{34})_2]\cdot 26\text{H}_2\text{O}$  (**2**) ( $2 \times 10^{-4}$  M) in HCl 0.1 M medium; scan rate: 10 mV/s. Insert: enlarged voltammogram of the negative potential domain.

Cyclic voltammetry studies on (**2**) in 0.1 M HCl revealed a less defined oxidation peak around 1.35-1.5 V and the associated reduction peak at 0.75 V which is assigned to the redox processes of  $\text{Co}^{\text{II}}$  ions.<sup>3</sup> As expected for the redox process of W(VI) centers in a polyoxotungstate, four wave pairs are located at -0.32(I), -0.40(II), -0.49(III) and 0.54(IV) V for the oxidation process and respectively -0.34(I'), -0.45(II'), -0.54(III') and 0.63(IV') for the reduction process.

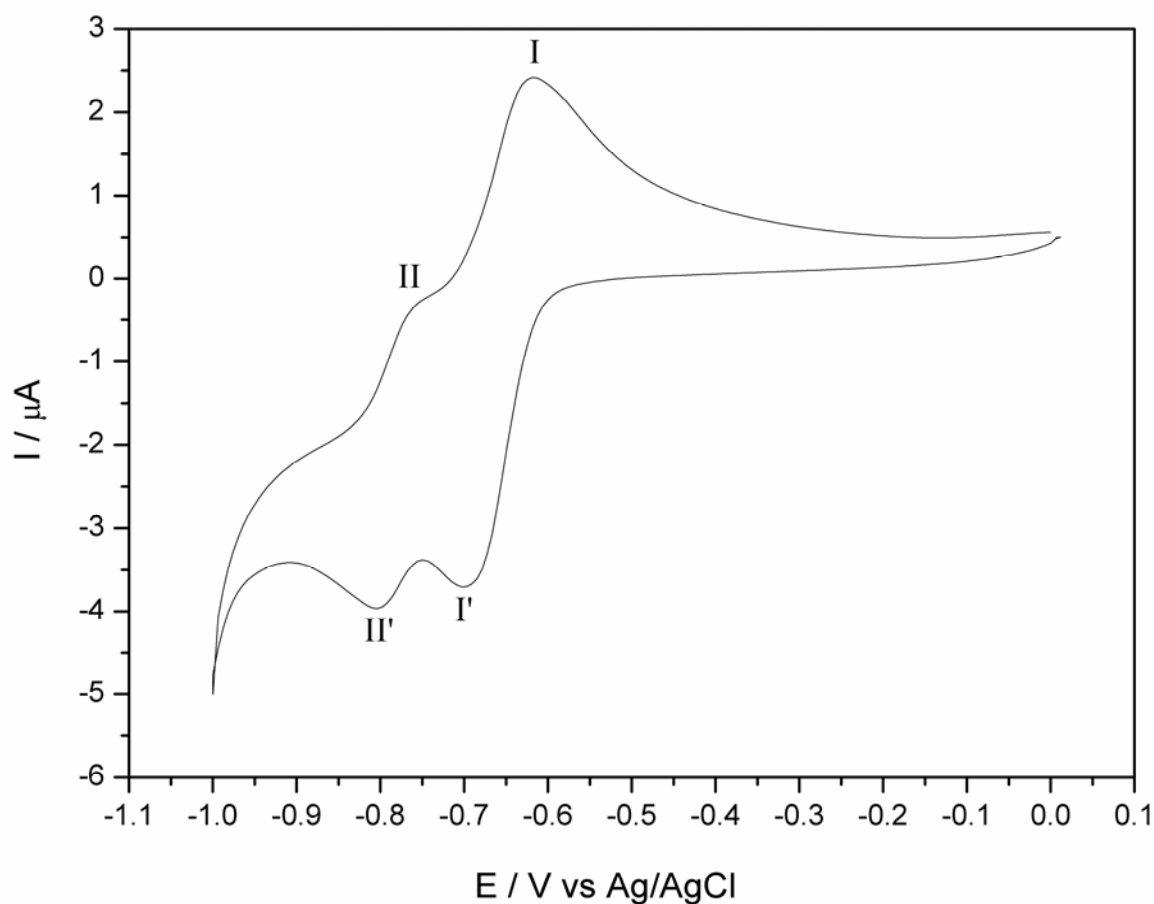


**Figure S16.** Cyclic voltammogram of  $\alpha\text{-K}_{11}\text{Na}_1[\text{Ni}_4(\text{H}_2\text{O})_2(\text{SiW}_9\text{O}_{34})_2]\cdot 27\text{H}_2\text{O}$  (**3**) ( $2 \times 10^{-4}$  M) in a pH 3 medium (0.5 M  $\text{Na}_2\text{SO}_4$  +  $\text{H}_2\text{SO}_4$  1 M); scan rate: 25 mV/s.

Cyclic voltammetry studies on (**3**) in sulfate medium at pH = 3 ( $\text{Na}_2\text{SO}_4$  0.5 M +  $\text{H}_2\text{SO}_4$  1M) confirm the presence of the  $\{\text{SiW}_9\text{O}_{34}\}$  precursor motif. At pH 3 two wave pairs at -0.62(I) – -0.75(II) V and -0.70(I') – -0.80(II') V are respectively assigned to the oxidation and the reduction processes of W(VI) centers.<sup>4</sup>

## 6. Electrospray Ionization Mass Spectrometry (ESI-MS)

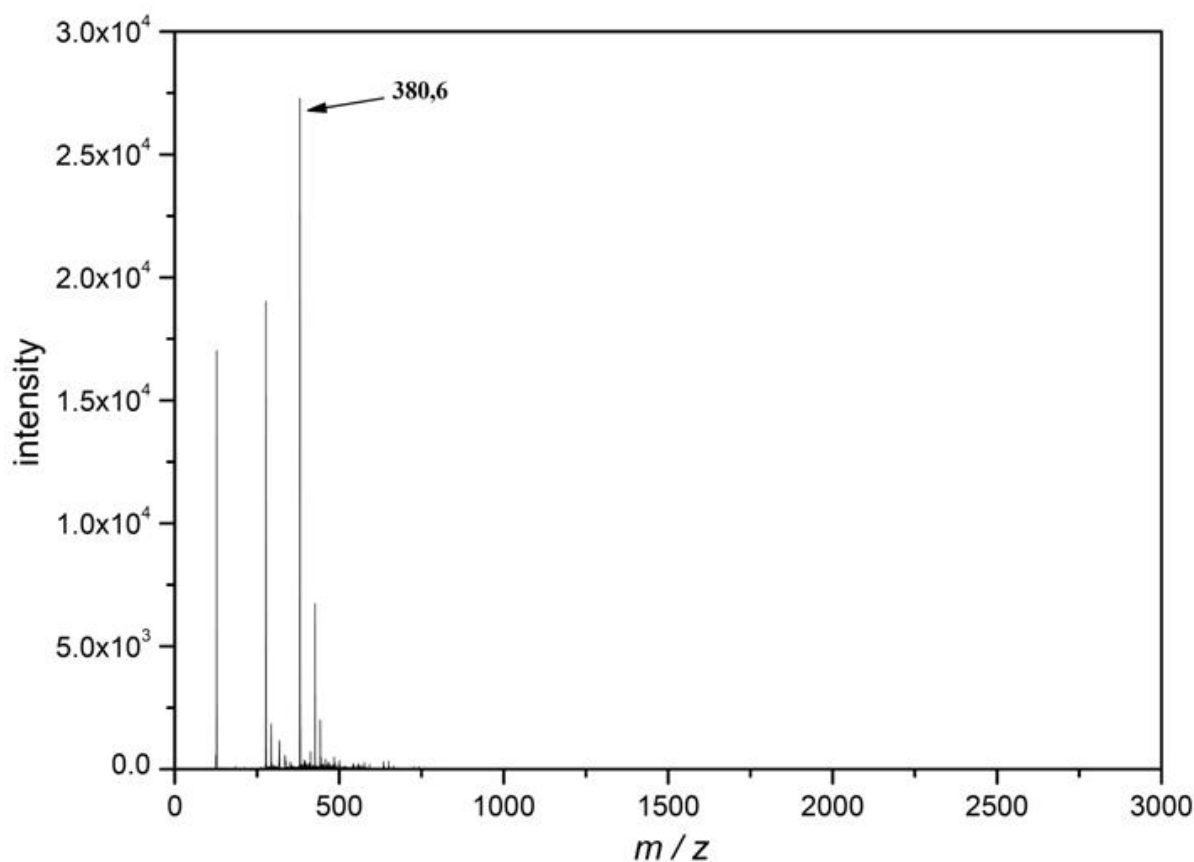


**Figure S17.** Negative ion mass spectrum showing  $[\{\text{Ru}_3\text{O}_3(\text{H}_2\text{O})\text{Cl}_2\}(\text{SiW}_9\text{O}_{34})]^{7-}$  in the  $m/z = 0\text{-}3000$  range. (1) was dissolved in NaI in methanol /  $\text{H}_2\text{O}$  (20:80). The ESI measurement was performed at 300 °C with azote as carrier gas at a flow of 6 L/min. Mass spectra were recorded on a Bruker HCT instrument and data were collected in negative mode. Parameters used: the end plate voltage was set to -500 V and the capillary to 4000 V. The sample solution was injected via a syringe pump directly connected the the ESI source (with a nebulizer pressure of 11 psi).

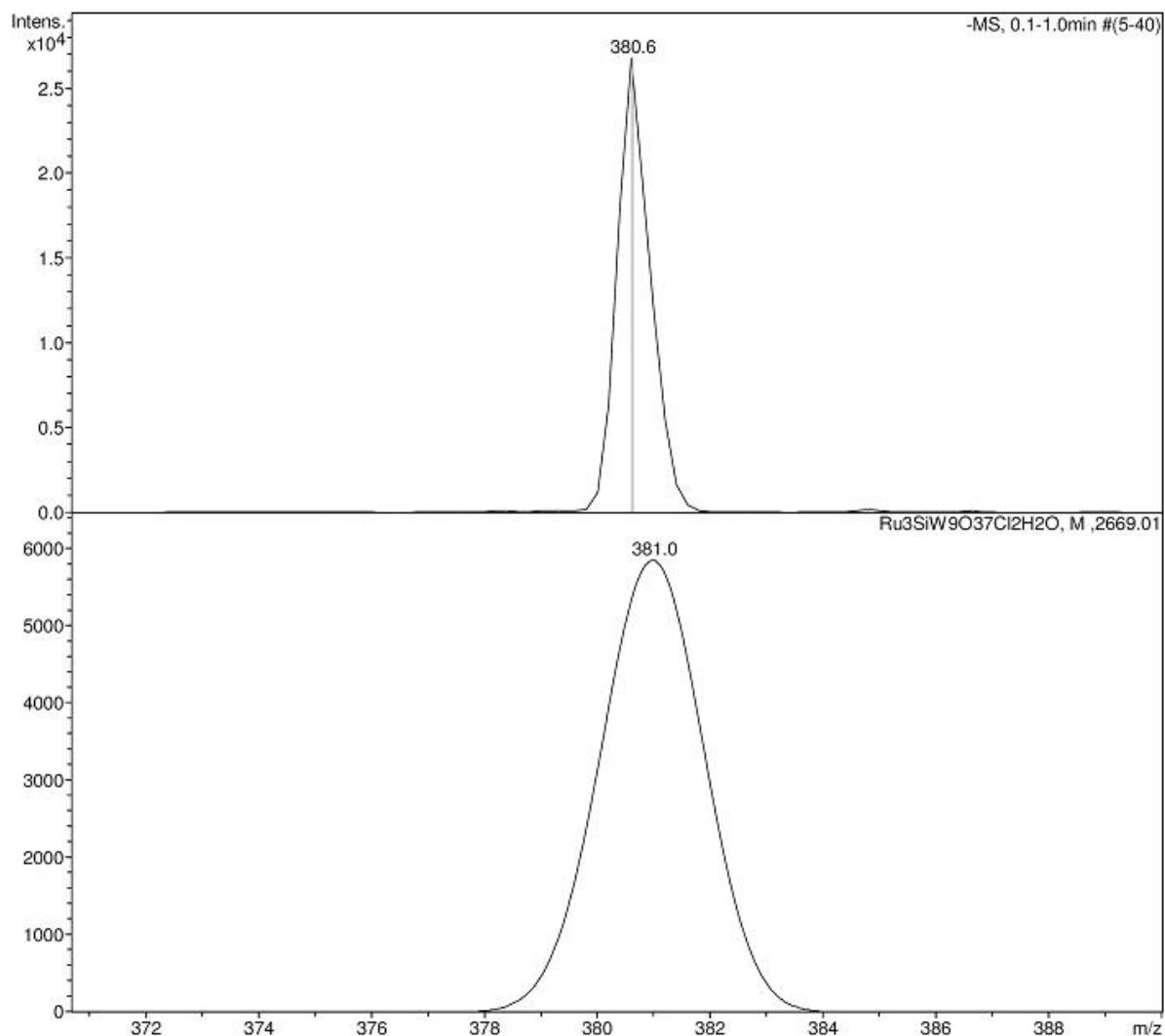


**Figure S18.** Experimental isotopic pattern (top) compared to the simulated isotopic pattern (bottom) of the  $[\{\text{Ru}_3\text{O}_3(\text{H}_2\text{O})\text{Cl}_2\}(\text{SiW}_9\text{O}_{34})]^{7-}$  anion present in (**1**). The observed isotopic pattern matches the theoretical isotope pattern calculated from the elemental composition of (**1**) using the ESI Compass 1.3 program.

## 7. Visible-light-driven water oxidation

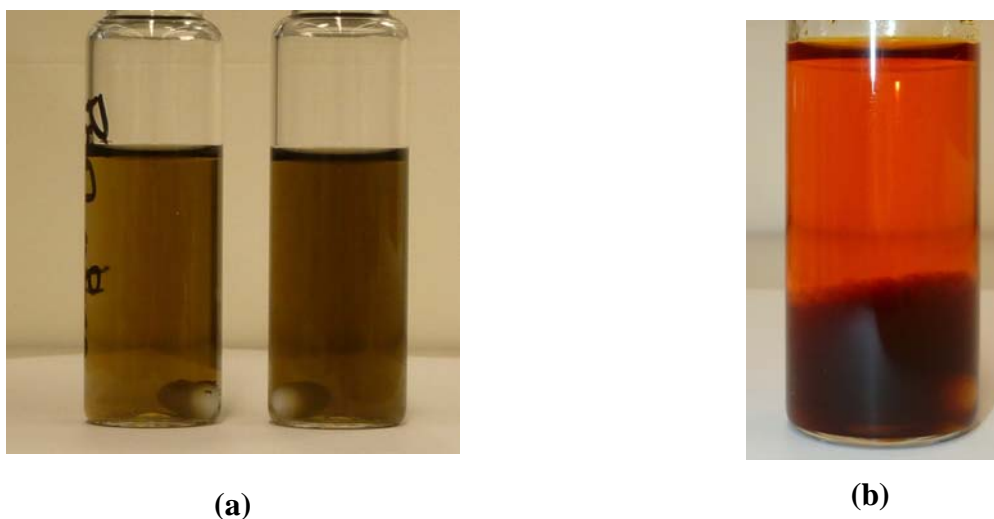


**Figure S19.** (a) Solution containing only **(1)** in  $\text{Na}_2\text{SiF}_6$  buffer after 3 h of illumination with a 470 nm LED; (b) formation of POM-photosensitizer complex from **(1)** and  $[\text{Ru}(\text{bpy})_3]^{2+}$ .

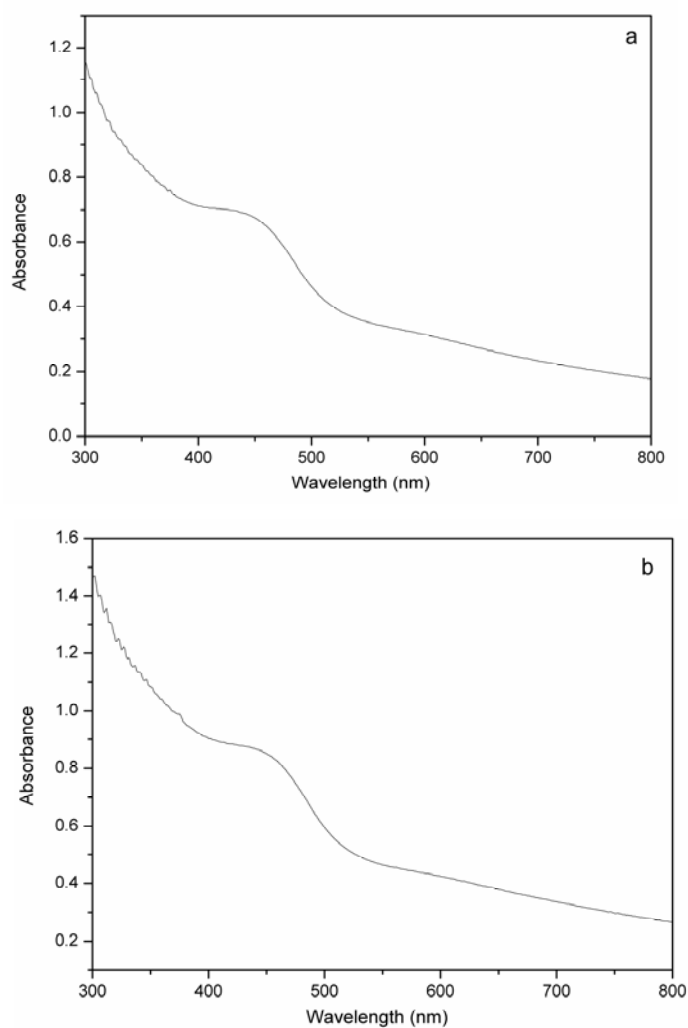


**Figure S20.** UV/vis spectra of mixtures shown in Fig. S19 above: (a) UV/vis spectrum of a solution containing only **(1)** in  $\text{Na}_2\text{SiF}_6$  buffer after 3 h of illumination with a 470 nm LED; (b) UV/vis spectrum of a solution containing **(1)** +  $\text{Na}_2\text{S}_2\text{O}_8$  in  $\text{Na}_2\text{SiF}_6$  buffer after 3 h of illumination with a 470 nm LED.

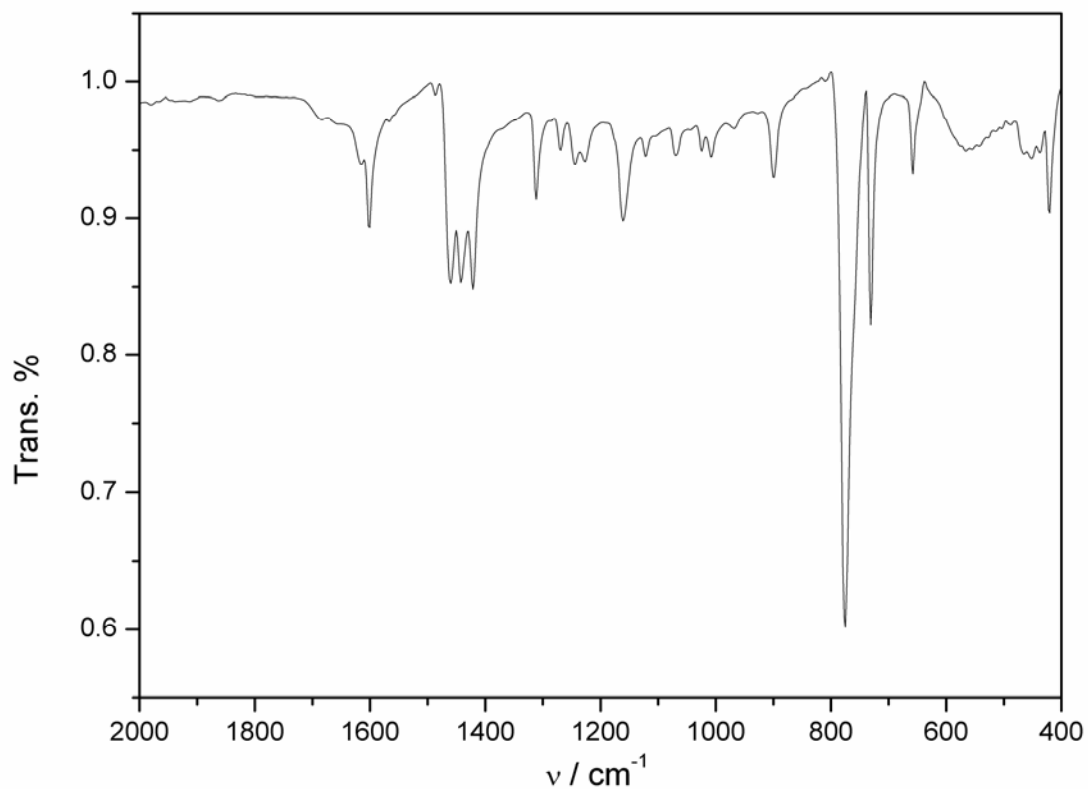


**Figure S21.** Solid state ATR FT-IR spectrum of the photosensitizer [Ru(bpy)<sub>3</sub>]Cl<sub>2</sub>.

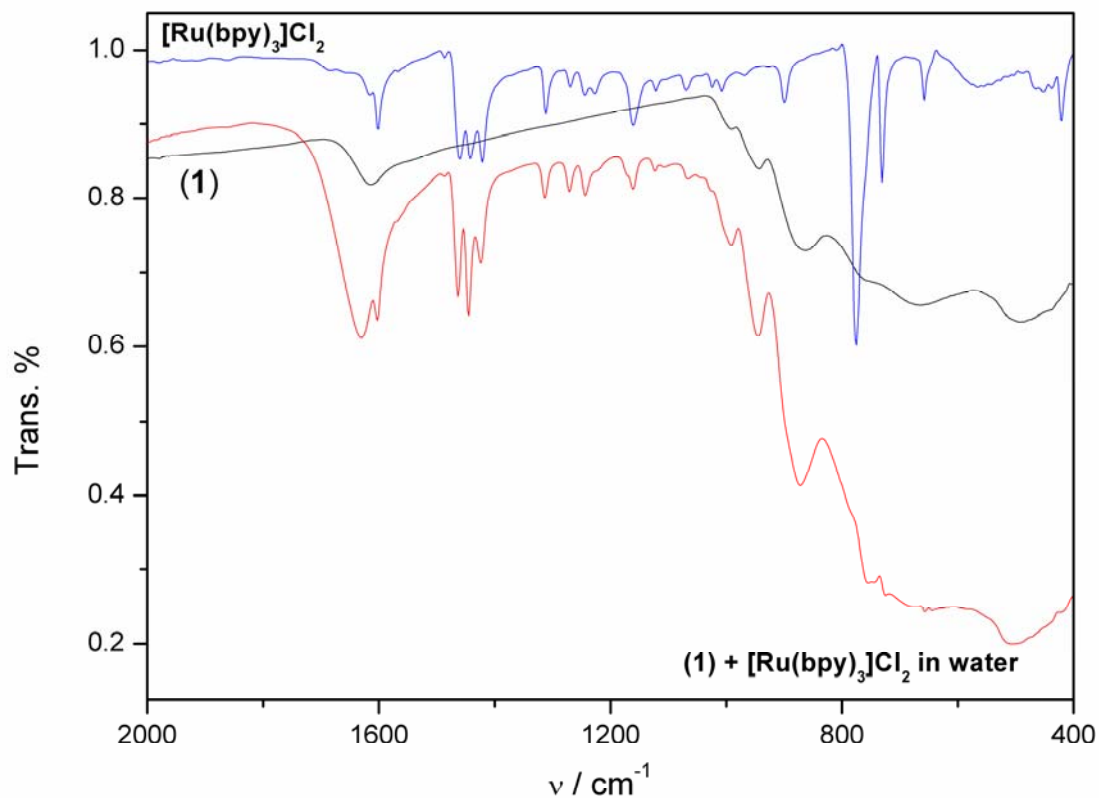


**Figure S22.** Solid state ATR FT-IR spectra comparison between POM (1) (red), precipitate formed by mixing the Ru(bpy)<sub>3</sub>Cl<sub>2</sub> and (1) in water (blue) and Ru(bpy)<sub>3</sub>Cl<sub>2</sub> (blue).

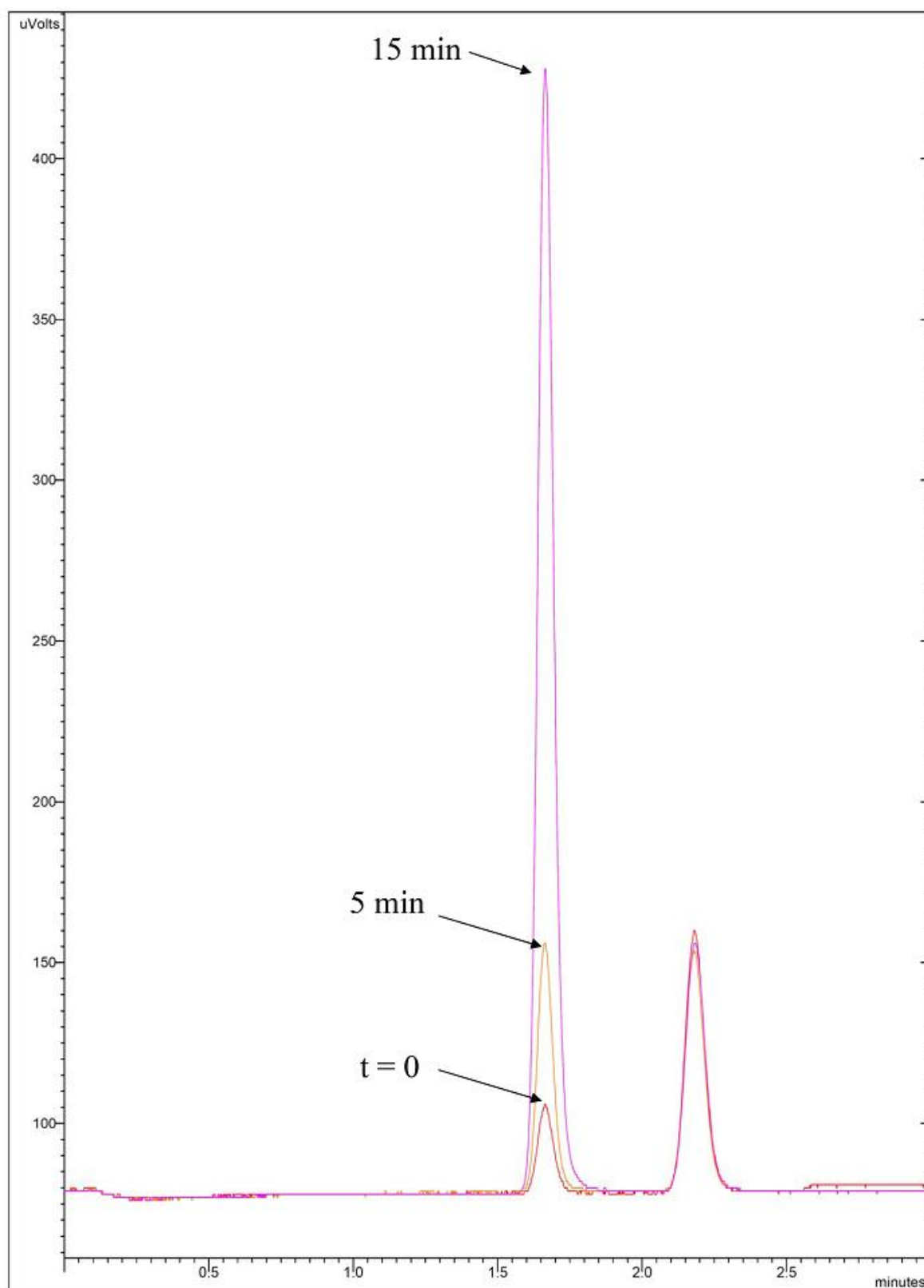


**Figure S23.** Representative GC trace chromatogram of a headspace of (1) after 15 min of illumination with a 470 nm LED under catalytic conditions (1 mM  $[\text{Ru}(\text{bpy})_3]\text{Cl}_2$ , 5 mM  $\text{Na}_2\text{S}_2\text{O}_8$ ,  $\text{Na}_2\text{SiF}_6$  buffer pH 5.8 (20 mM) and 50  $\mu\text{M}$  of (1).  $\text{N}_2$  area is in line with manual injection.<sup>5</sup>

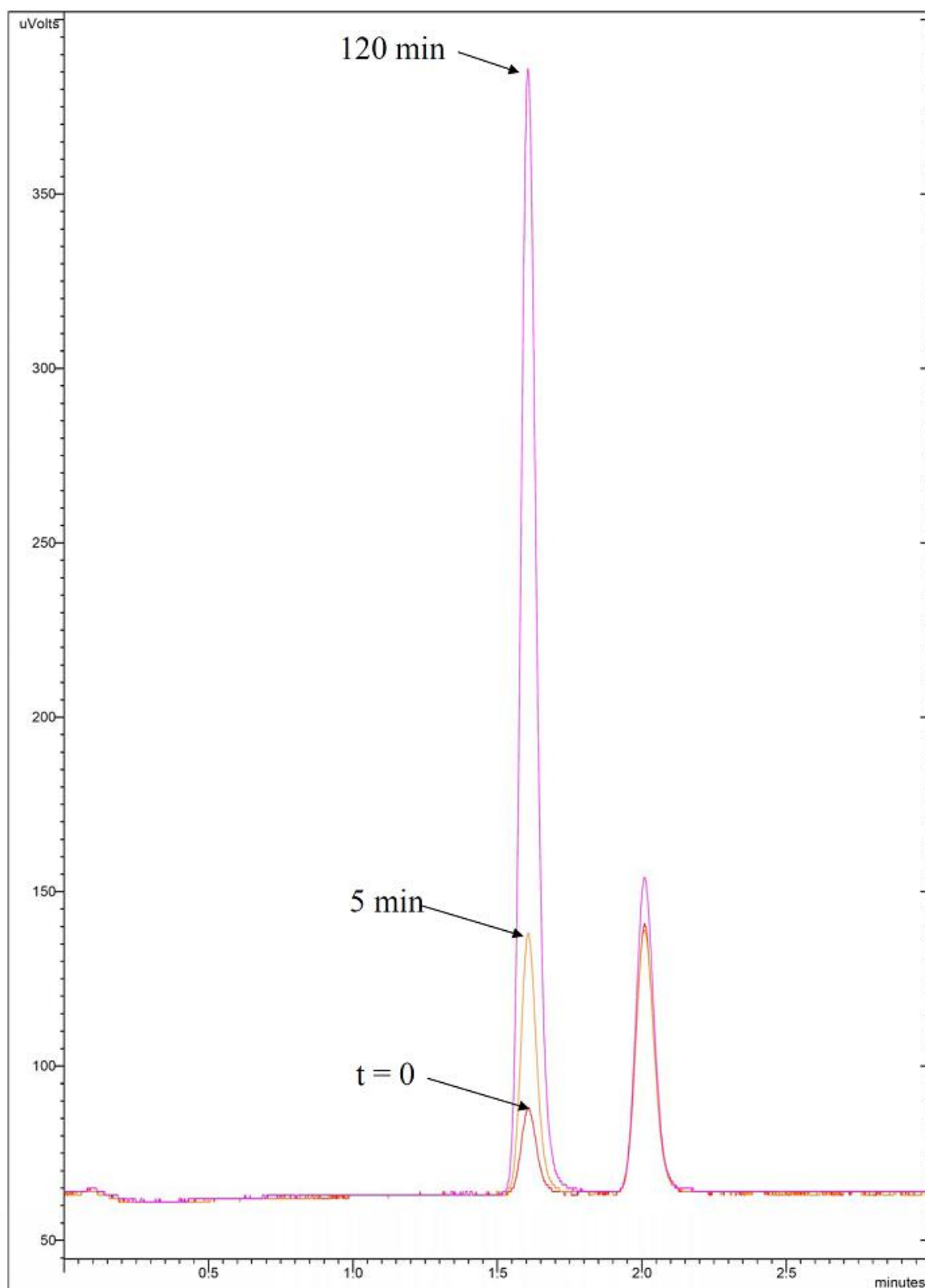


**Figure S24.** Representative GC trace chromatogram of a headspace of the catalytic suspension formed from **(1)** (after 15 min, see Fig. S22) and dispersed in a fresh catalytic solution containing 1 mM  $[\text{Ru}(\text{bpy})_3]\text{Cl}_2$  and 5 mM  $\text{Na}_2\text{S}_2\text{O}_8$ ,  $\text{Na}_2\text{SiF}_6$  buffer pH 5.8 (20 mM) and stopped after 120 min.  $\text{N}_2$  area is in line with manual injection.<sup>5</sup>

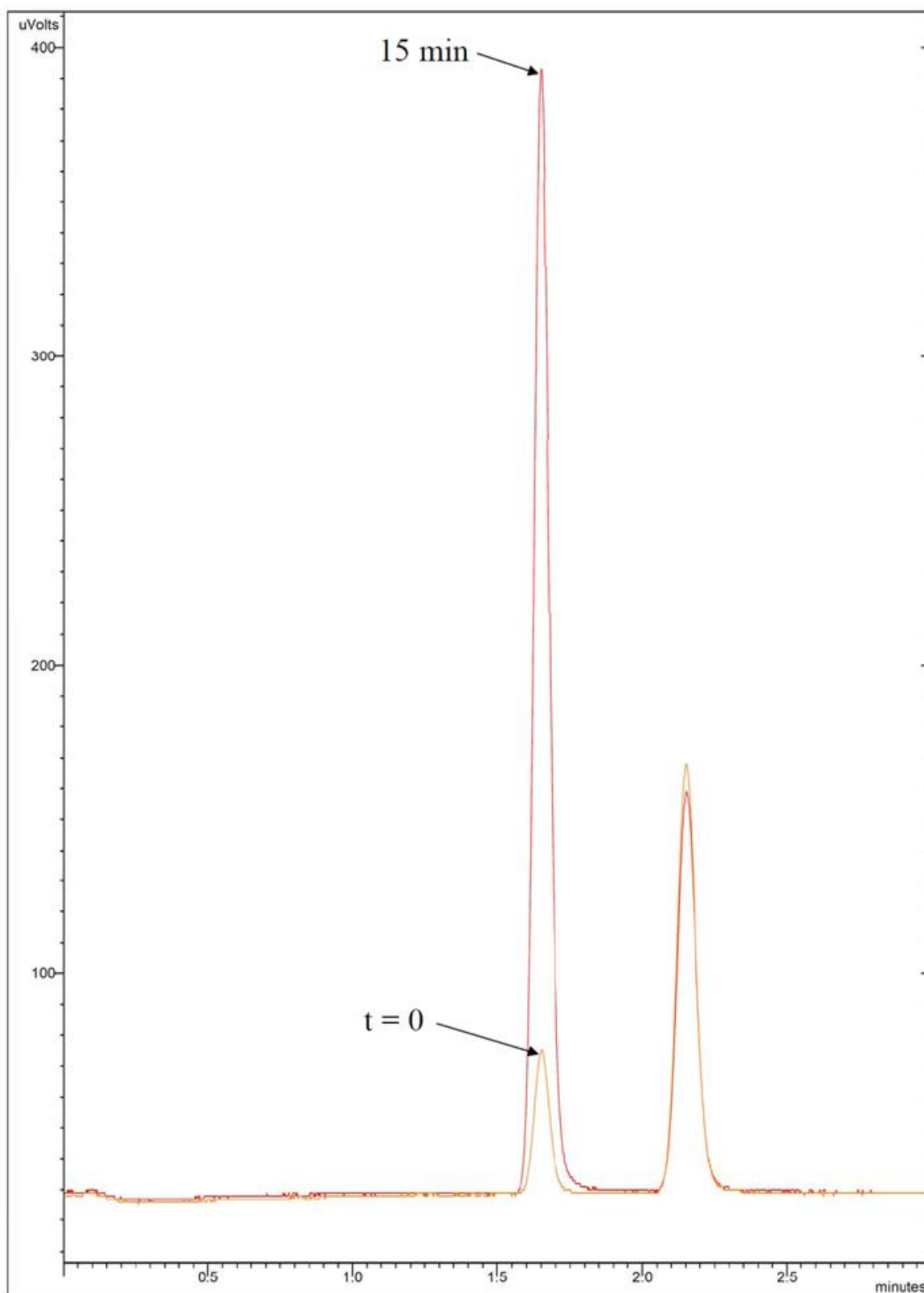


**Figure S25.** Representative GC trace chromatogram of a headspace of **(2)** after 15 min of illumination with a 470 nm LED under catalytic conditions (1 mM  $[\text{Ru}(\text{bpy})_3]\text{Cl}_2$ , 5 mM  $\text{Na}_2\text{S}_2\text{O}_8$ ,  $\text{Na}_2\text{SiF}_6$  buffer pH 5.8 (20 mM), and 2.4 mg of **(2)**).  $\text{N}_2$  area is in line with manual injection.<sup>5</sup>

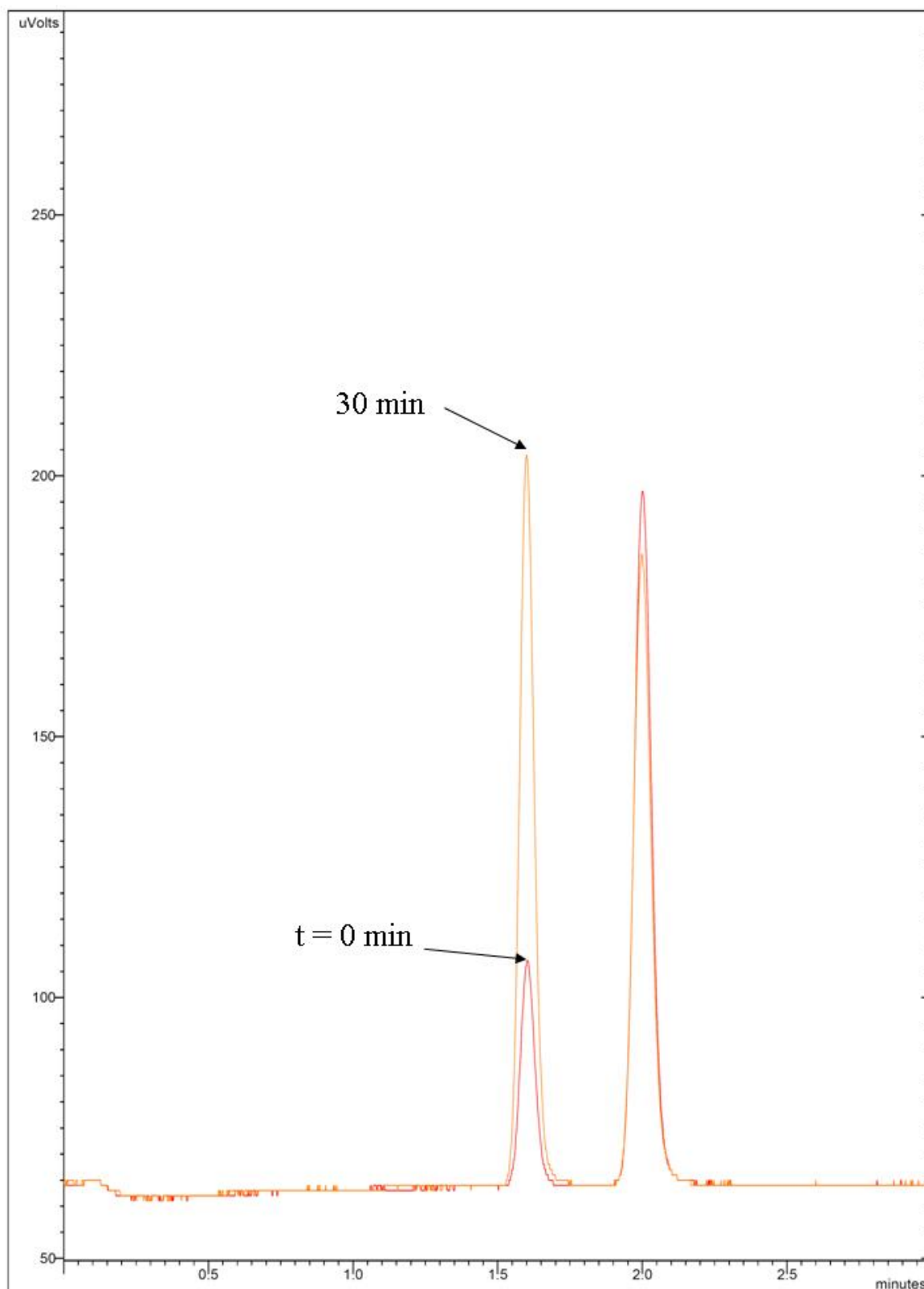


**Figure S26.** Representative GC trace chromatogram of a headspace of the catalytic suspension formed from **(2)** (after 15 min, see Fig. S24) and dispersed in a fresh catalytic solution containing 1 mM  $[\text{Ru}(\text{bpy})_3]\text{Cl}_2$  and 5 mM  $\text{Na}_2\text{S}_2\text{O}_8$ ,  $\text{Na}_2\text{SiF}_6$  buffer pH 5.8 (20 mM) and stopped after 120 min.  $\text{N}_2$  area is in line with manual injection.<sup>5</sup>

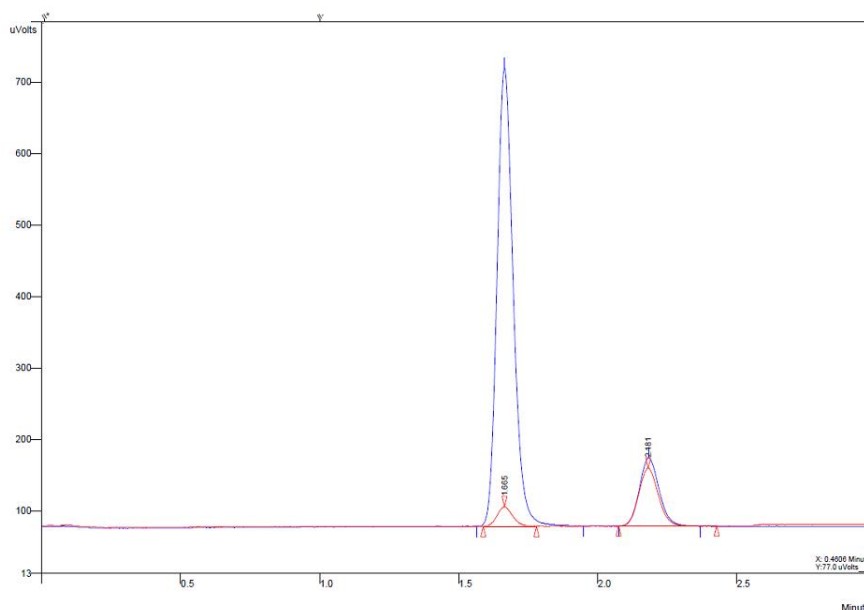


**Figure S27.** Representative GC trace chromatogram of a headspace in the reaction of water oxidation with 46  $\mu\text{M}$  of **(1)**, 1mM of  $\text{Ru}(\text{bpy})_3\text{Cl}_2$  and 5 mM of  $\text{Na}_2\text{S}_2\text{O}_8$  in  $\text{Na}_2\text{SiF}_6$  buffer media (20 mM, pH 5.8). Red: blank measurement after 30 min of He flow (in line with a manual injection).<sup>5</sup> Blue:  $\text{O}_2$  evolution after 80 min (in very good agreement with a constant quantity of  $\text{N}_2$ ).

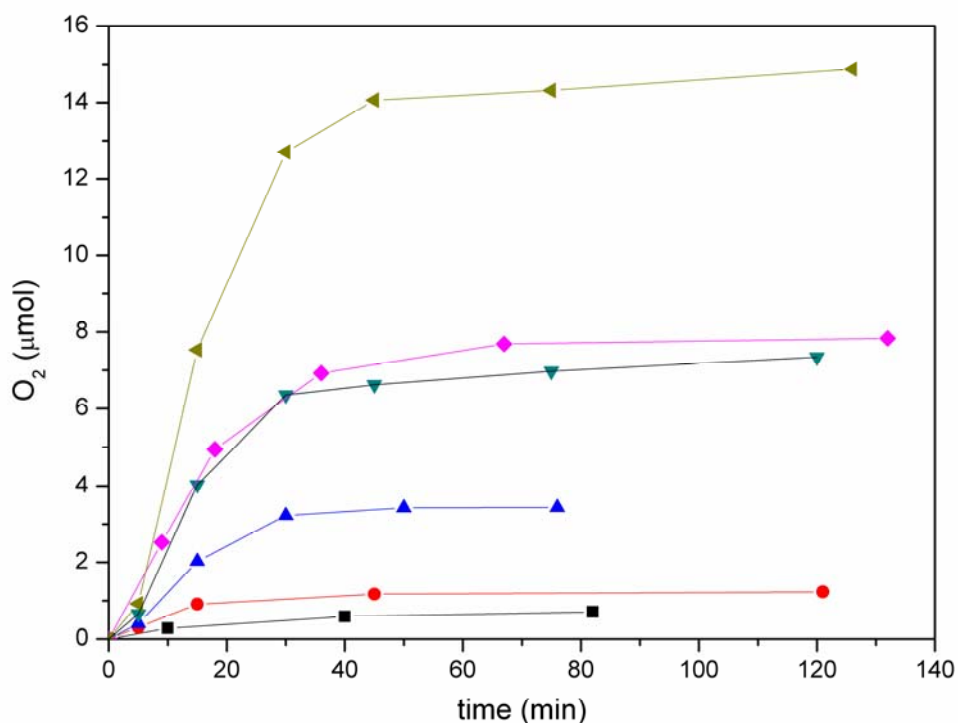


**Figure S28.** Full kinetic data of light induced  $\text{O}_2$  formation from water oxidation with persulfate as a sacrificial electron acceptor. Conditions: LED lamp, 470 nm; 1 mM  $[\text{Ru}(\text{bpy})_3]\text{Cl}_2$ , 5 mM  $\text{Na}_2\text{S}_2\text{O}_8$ ,  $\text{Na}_2\text{SiF}_6$  buffer pH 5.8 (20 mM), 10  $\mu\text{M}$  **(1)** ( $\blacksquare$ ), 16  $\mu\text{M}$  **(1)** ( $\bullet$ ), 21  $\mu\text{M}$  **(1)** ( $\blacktriangle$ ), 30  $\mu\text{M}$  **(1)** ( $\blacktriangledown$ ), 31  $\mu\text{M}$  **(1)** ( $\blacklozenge$ ), 50.00  $\mu\text{M}$  **(1)** ( $\blacktriangleleft$ ); total solution volume in each reaction: 13 mL.

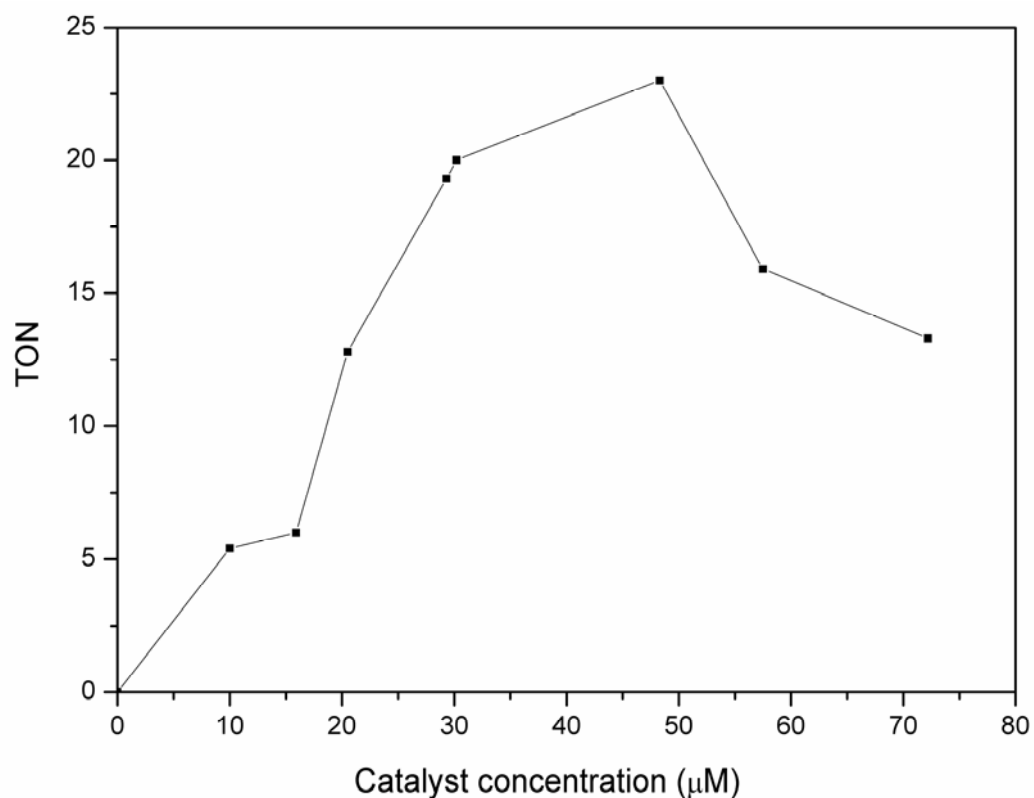


**Figure S29.** Turnover number (TON) vs. concentration of  $\alpha$ - $\text{K}_6\text{Na}[\{\text{Ru}_3\text{O}_3(\text{H}_2\text{O})\text{Cl}_2\}(\text{SiW}_9\text{O}_{34})\cdot 17\text{H}_2\text{O}$  (**1**).



**Figure S30.** Left: gas chromatograph (Varian CP-3800) for recording chromatograms and monitoring  $\text{O}_2$  evolution during water oxidation; right: illumination of the reaction vessel by the light of a 470 nm high flux LED (Rhopoint Components LTD).

## 8. References

- 
- 1 J. A. F. Gamelas, H. M. Carapuça, M. S. Balula, D. V. Schlindwein, F. G. Figueiras, V. S. Amaral and A. M. V. Cavaleiro, *Polyhedron*, 2010, **29**, 3066.
  - 2 a) K. Filipek, *Inorg. Chim. Acta*, 1995, **231**, 237; b) M. Sadakane, D. Tsukuma, M. H. Dickman, B. S. Bassil, U. Kortz, M. Higashijima and W. Ueda, *Dalton Trans.*, 2006, 4271.
  - 3 B. S. Bassil, S. Nellutla, U. Kortz, A. C. Stowe, J. Van Tol, N. S. Dalal, B. Keita and L. Nadjo, *Inorg. Chem.*, 2005, **44**, 2659.
  - 4 X. Zhao, Y. G. Li, Y. H. Wang and E. B. Wang, *Transition Metal Chem.*, 2008, **33**, 323.
  - 5 Y. V. Geletii, B. Botar, P. Kögerler, D. A. Hillesheim, D. G. Musaev and C. L. Hill, *Angew. Chem. Int. Ed.*, 2008, **47**, 3896.